AD-A220 237

(4)

Technical Document 1739
December 1989

Radar Clutter via Waveguide Methods

R. A. Pappert

NAVAL OCEAN SYSTEMS CENTER
San Diego, California 92152-5000

J. D. FONTANA, CAPT, USN
Commander

R. M. HILLYER
Technical Director

ADMINISTRATIVE INFORMATION

This project was carried out by the Ionospheric Branch, Code 542, of the Naval Ocean Systems Center, San Diego, CA, with funding provided by the Office of Naval Technology, Arlington, VA 22217, under program element 0602435N.

Released by
J. A. Ferguson, Head
Ionospheric Branch

Under authority of
J. H. Richter, Head
Ocean and Atmospheric
Sciences Branch

ACKNOWLEDGMENT

The author wishes to thank Ms. L. R. Hitney for her programming assistance.

FS

Abstract

Recent backscatter results generated by Tappert, using parabolic equation and Monte Carlo methods, afford an excellent opportunity to assess the adequacy of concepts such as shadowing and surface tilting often used in concert with ray concepts for line of sight backscatter calculations. In this study, results of first order scatter from rough surfaces are used in conjunction with waveguide formalism to calculate clutter from distant ranges in tropospheric waveguide environments. Comparisons are made with Tappert's results at 9.6 GHz for the standard atmosphere, and for 14 and 28 m evaporation ducts. Results apply to wind speeds of 10, 20, 30 and 40 knots. Averaged backscattered signals calculated by the two methods, for a transmitter altitude of 25 m, agree to within about ± 10 dB. This is considered surprisingly good agreement in view of the many uncertainties and approximations involved in the calculations.

1.0 INTRODUCTION

Tappert*, in a recent study, has used parabolic equation and Monte Carlo methods to calculate sea clutter for a variety of sea states and evaporation ducts. In particular, he has carried the clutter calculations well beyond the normal horizon. An interesting question is whether waveguide methods might also be useful for such calculations? An immediate response would quite possibly be no, since waveguide modes are generally complex and there would seemingly be no way of accommodating such quantities within the conventional framework of line of sight rough surface scatter which deals with real angles of incidence. Nevertheless, Tappert's work has motivated the present exploratory study of sea clutter via normal mode methods.

In the following section, abundant useage is made of first order scatter theory from a rough surface as developed by Ulaby, Moore and Fung[1]. In particular, first order theory is used in conjunction with normal mode formalism. As will be shown, this leads to the physically satisfying result of the backscattered power falling off inversely with range along with an attenuation associated with two way transit between transmitter and receiver. First order scatter theory is applied to capillary waves on an otherwise flat surface. In actuality, the capillary waves ride on longer wavelength waves which scatter energy out of the specular direction and thereby augment modal attenuation rates. Approximate allowance for this effect is made by assuming the surface obeys Gaussian statistics and by using Kirchhoff theory to modify the smooth surface ground reflection coefficient.[2,3] Additionally, the long wavelength waves effect a tilting of the surface, thereby altering the local angle of incidence. Moreover, the longwaves shadow portions of the scattering surface. Awareness of these effects has given rise to the so called "composite surface model" which has been used extensively for within the line of sight calculations in non-ducting environments.[1,4-6] Though lacking in rigor, these long

* This citation refers to a hand-written report prepared by Dr. F. D. Tappert of the University of Miami, while working at NOSC during the summer of 1989. For further information, please contact R. A. Pappert, Code 542, or H. V. Hitney, Code 543, Naval Ocean Systems Center, San Diego, CA.

wavelength effects are treated in section III by the same methods conventionally used for line of sight calculations in non-ducting environments.

Comparisons with Tappert's results are given in section IV and a general discussion in section V concludes the paper.

2.0 BRAGG SCATTER

In the following development, a rectangular coordinate system is used with x the range variable, z the altitude variable with z = 0 corresponding to ground level. A thin vacuum layer is assumed immediately above a random rippled, but otherwise flat, ocean surface and the polarization is taken to be horizontal. Ulably et al.[1] have treated in considerable detail the problem of first order scatter from such a surface for plane wave incidence. Their result for the spectral decomposition of the scattered field due to a unit amplitude incident plane wave in the x-z plane is (a time dependence $\exp(j\omega t)$ is assumed)

$$E_y^{(s)} = \frac{1}{2\pi} \int\int_{-\infty}^{\infty} U_y(k_x, k_y) \exp(jk_x x + jk_y y - jk_z z) dk_x dk_y, \tag{1}$$

where

$$U(k_x, k_y) = -h(k_x, k_y) f, \tag{2}$$

$$h(k_x, k_y) = (k_z k_z' + k_x^2)/D, \tag{3}$$

$$k_z = (k^2 - k_x^2 - k_y^2)^{1/2}, \quad k_z' = (k^2 n_g^2 - k_x^2 - k_y^2)^{1/2}, \tag{4}$$

$$D = (k_z + k_z')(k_x^2 + k_y^2 + k_z k_z'), \tag{5}$$

$$f = jk^2(n_g^2-1)(1+\bar{R}_\perp)z(k_x+kS,k_y), \tag{6}$$

$$n_g^2 = \frac{\sigma}{i\omega\epsilon_0} + \frac{\epsilon}{\epsilon_0}, \tag{7}$$

$$\bar{R}_\perp = \frac{C - (n_g^2-S^2)^{1/2}}{C + (n_g^2-S^2)^{1/2}}, \tag{8}$$

$$z(k_x,k_y) = \frac{1}{2\pi}\int_{-\infty}^{\infty}\int z(x,y)\exp(-jk_x-jk_y y)dxdy, \tag{9}$$

$$S = \sin\theta,\ C = \cos\theta, \tag{10}$$

θ = plane wave angle of incidence, (11)

k = free space wave number, (12)

ω = circular frequency, (13)

σ = ground conductivity, $\frac{\epsilon}{\epsilon_0}$ = ground dielectric constant, (14)

z(x,y) = random function defining rippled surface. (15)

Unless otherwise specified, MKS units are assumed. In the above $\bar{R}_\perp$ is the Fresnel reflection coefficient for horizontal polarization. Signs of the square roots which occur in the above equations are taken in such a way as to assure either upward propagation or evanescence for z>o and downward propagation for z<o.

The broadside electric field, in the assumed vacuum region bordering the surface, generated by a horizontal electric dipole, $\vec{p}$, may be written as the following modal decomposition[7] (kx>>1 is assumed)

$$E_y^{inc} \simeq \frac{A}{\sqrt{x}} \sum_m \lambda_m e_{ym}(z_T)\exp(-jkS_m x)(\exp(jkC_m z)+ \bar{R}_{\perp m}\exp(-jkC_m z)), \tag{16}$$

where m is a modal index, $e_{ym}(z_T)$ is the modal height gain at the transmitter and is normalized to $1 + \bar{R}_{\perp m}$ at the ground. The excitation factor, λ_m, is given by

$$\lambda_m = \frac{1}{\left(\bar{R}_\perp \frac{\partial F}{\partial \theta}\right)_m} , \tag{17}$$

where the modal function, F, is

$$F = 1 - \bar{R}_\perp R_\perp , \tag{18}$$

and R is the plane wave reflection coefficient for horizontal polarization from everything above z = 0 with vacuum below it. The constant A is given by

$$A = \frac{p}{4\pi\epsilon_o} \pi k^3 \left(\frac{2}{\pi k}\right)^{1/2}\exp(j\pi/4). \tag{19}$$

To good approximation, the factor $1+\bar{R}_\perp$ which appears in Eq.(6) may be written as

$$1 + \bar{R}_\perp \simeq \frac{2C}{(n_g^2-1)^{1/2}}. \tag{20}$$

The amplitude at the surface, of the incident plane wave associated with the dipole generated field, is interpreted to be the factor, apart from the range dependent exponential term, which multiplies the $\exp(jkC_m z)$ term in Eq.(16). Combining this factor with Eq.(1) and using Eqs.(9) and (20) yields

$$E_y^{(s)} \simeq -\frac{jAk^2(n_g^2-1)^{1/2}}{2\pi^2} \iiint_{-\infty}^{\infty} h(k_x,k_y) z(x',y') \exp(jk_x(x-x')+jk_y(y-y')-jk_z(z-z'))$$

$$\cdot \left(\frac{1}{x'}\right)^{1/2} \sum_m C_m \lambda_m \exp(-jkS_m x') e_{ym}(z_T)\, dk_x dk_y dx' dy'. \tag{21}$$

To arrive at Eq.(21) it has been tacitly assumed that the incident radiation is an outward propagating pulse with x' much greater than the pulse length so that the geometrical factor $1/\sqrt{x'}$ has been taken to be constant over the illuminated area.

The integrals over k_x and k_y are now transformed to cylindrical coordinates via the transformations

$$k_x = k\sin\theta\cos\phi,\ k_y = k\sin\theta\sin\phi, \tag{22}$$

$$k_z = k\cos\theta,\ dk_x dk_y = k^2\sin\theta\cos\theta d\phi, \tag{23}$$

$$x-x' = r\cos\phi_r,\ y-y' = r\sin\phi_r. \tag{24}$$

Also, to good approximation

$$h(k_x,k_y) \simeq \frac{1}{k_z'} \simeq \frac{1}{k(n_g^2-1)^{1/2}}, \tag{25}$$

so that the scattered field becomes

$$E_y^{(s)} \simeq -j\frac{Ak^3}{2\pi^2} \iint_{-\infty}^{\infty} dx' dy' \frac{z(x',y')}{\sqrt{x'}} \sum_m C_m \lambda_m \exp(-jkS_m x') e_{ym}(z_T) \int_o^{\frac{\pi}{2}+j\infty} SC\exp(-jkCz)d\theta$$

$$\cdot \int_o^{2\pi} \exp(jkrS\cos(\phi-\phi_r))d\phi. \qquad (26)$$

The upper limit of the theta integration has been determined by the condition $k_z \rightarrow -j\infty$ as $k_x, k_y \rightarrow \infty$. The integral over ϕ is proportional to the zero order Bessel function, J_o, so that the scattered field becomes

$$E_y^{(s)} \simeq -j\frac{Ak^3}{\pi} \iint_{-\infty}^{\infty} dx' dy' \frac{z(x',y')}{\sqrt{x'}} \sum_m C_m \lambda_m \exp(-jkS_m x') e_{ym}(z_T) \int_o^{\frac{\pi}{2}+j\infty} SCJ_o(krS)\exp(-jkCz)d\theta. \qquad (27)$$

The integral over θ can be written in terms of an integral over the Hankel function of the second kind, $H_o^{(2)}$. Effecting that transformation allows for the scattered field to be written as

$$E_y^{(s)} \simeq -j\frac{Ak^3}{2\pi} \iint_{-\infty}^{\infty} dx' dy' \frac{z(x',y')}{\sqrt{x'}} \sum_m C_m \lambda_m \exp(-jkS_m x') e_{ym}(z_T) \int_{-\frac{\pi}{2}-j\infty}^{\frac{\pi}{2}+j\infty} SCH_o^{(2)}(krS)\exp(-jkCz)d\theta. \qquad (28)$$

Equation (28) represents the scattered field in the thin vacuum region in the neighborhood of the surface without full allowance for stratification. This field is generalized to fully apply to a stratified media by allowing for the repeated reflections which occur between ground and the stratified media. To make this more precise, a vacuum will be assumed between ground level and an infinitesimal level α. The plane wave reflection coefficient from the

ground is simply the $\bar{R}_{\perp}$ coefficient already introduced. The plane wave reflection coefficient from everything above level α and referenced to level α will be denoted by $\bar{R}_{\perp\alpha}$. The infinite sum of reflections associated with the process whereby the upgoing wave from the surface goes directly to the receiver at $z<\alpha$ or first reflects off the upper stratification and then off the ground to the receiver etc. leads to the expression

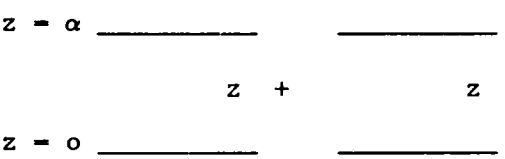

$$\exp(-jkCz)/(1-\bar{R}_{\perp}\, R_{\perp\alpha}\exp(-2jkC\alpha)). \quad (29)$$

The infinite sum of reflections associated with the process whereby the upgoing wave first reflects from the stratification to the receiver and then from the stratification to the ground and once again from the stratification to the receiver etc. yields

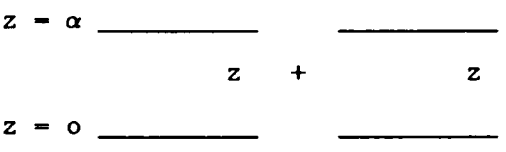

$$R_{\alpha}\exp(-jkC(2\alpha-z))/(1-\bar{R}_{\perp}\, R_{\perp\alpha}\exp(-2jkC\alpha)). \quad (30)$$

When the z dependent term in the theta integral of Eq.(28) is replaced by the sum of Eqs. (29) and (30), the limit α, $z\to 0$ taken and the theta integral evaluated by residue theory there results

$$E_y^{(s)} \simeq Ak^3 \int_{-\infty}^{\infty}\int dx'\,dy' \frac{z(x',y')}{\sqrt{x'}} \sum_m C_m\lambda_m \exp(jkS_m x')\, e_{ym}(z_T) \sum_n S_n C_n \lambda_n H_o^{(2)}(kS_n r)(1+\bar{R}_{\perp m}). \quad (31)$$

The term $1 + \bar{R}_{\perp n}$ is simply the modal height gain at the ground. For backscatter at the transmitter location, the $1 + \bar{R}_{\perp n}$ term need only to be replaced by the modal height gain $e_{yn}(z_T)$ with the understanding that $e_{yn}(0) = 1 + \bar{R}_{\perp n}$. Making this replacement as well as the asymptotic replacement for $H_o^{(2)}$ and noting that $S_n \simeq 1$, Eq.(31) becomes

$$E_y^{(s)} \simeq B \int_{-\infty}^{\infty} dx' dy' \frac{z(x',y')}{\sqrt{x'}} \sum_m C_m \lambda_m \exp(-jkS_m x') e_{ym}(z_T) \frac{1}{\sqrt{r}} \sum_n C_n \lambda_n \exp(-jkS_n r) e_{yn}(z_T), \tag{32}$$

where

$$B = \frac{jp}{4\pi\epsilon_o} 2k^5. \tag{33}$$

It can further be shown that if $k\Delta\phi\bar{y} \ll 1$ where $\Delta\phi$ is a measure of the angular beam pattern (assumed to be on the order of hundreths of a radian) and $\bar{y}$ a measure of the correlation length of the capillary waves (presumed to be on the order of centimeters) then to good approximation r can be replaced by x' in Eq.(32) so that

$$E_y^{(s)} \simeq B \int_{-\infty}^{\infty} dx' dy' \frac{z(x',y')}{x'} \sum_m C_m \lambda_m \exp(-jkS_m x') e_{ym}(z_T) \sum_n C_n \lambda_n \exp(-jkS_n x') e_{yn}(z_T). \tag{34}$$

Equation (34) is the y component of the electric field at the receiver. To calculate the Poynting flux the H_z field is also required. From Maxwell's curl$\vec{E}$ equation the H_z field is

$$H_z^{(s)} \simeq - E_y^{(s)}/\eta, \tag{35}$$

where η is the free space impedance, $\sqrt{\mu_o/\epsilon_o}$, with μ_o the freespace permeability and ϵ_o the free space permittivity. The time averaged Poynting flux is (the * denotes the complex conjugate and the braces, <>, an ensemble average).

$$\frac{1}{2} < E_y^{(s)} H_z^{(s)*} > = - \frac{|B|^2}{2\eta} \iiint_{-\infty}^{\infty} dx' dy' dx'' dy'' <z(x',y')z(x'',y'')> \frac{1}{x' x''}$$

$$\cdot \sum\sum\sum\sum_{mnpq} C_m C_n C_p^* C_q^* \lambda_m \lambda_n \lambda_p^* \lambda_q^* \exp(jk((S_n+S_m)x' - (S_p^*+S_q^*)x''))$$

$$\cdot e_{ym}(z_T) e_{yn}(z_T) e_{yp}^*(z_T) e_{yq}^*(z_T). \qquad (36)$$

The space integrals in Eq.(36) are next transformed as follows

$$\bar{x} = x'' - x', \quad \bar{y} = y'' - y', \quad X = \frac{1}{2}(x'+x''), \quad Y = \frac{1}{2}(y'+y''), \qquad (37)$$

$$dx' dy' dx'' dy'' = d\bar{x} d\bar{y} dX dY. \qquad (38)$$

Assuming $z(x',y')$ is a homogeneous random function, the ensemble average $<z(x',y')z(x'',y'')>$ simply becomes $\rho(\bar{x},\bar{y})$ where ρ is the surface correlation function. Equation (38) then transforms to

$$\frac{1}{2} < E_y^{(s)} H_z^{(s)*} > = - \frac{|B|^2}{2\eta} \iiint_{-\infty}^{\infty} d\bar{x} d\bar{y} dX dY \; \rho(\bar{x},\bar{y}) \frac{1}{(X+\frac{1}{2}\bar{x})(X-\frac{1}{2}\bar{x})}$$

$$\cdot \sum\sum\sum\sum_{mnpq} C_m C_n C_p^* C_q^* \lambda_m \lambda_n \lambda_p^* \lambda_q^* \exp(-jk((S_n+S_m)(X+\tfrac{1}{2}\bar{x}) - (S_p^*+S_q^*)(X-\tfrac{1}{2}\bar{x})))$$

$$\cdot\, e_{ym}(z_T)e_{yn}(z_T)e^*_{yp}(z_T)e^*_{yq}(z_T)\,. \tag{39}$$

Now $\bar{x}$ is on the order of the surface correlation length (i.e., on the order of centimeters). Therefore, it is negligible relative to X (which is many kilometers) in the denominator terms of Eq.(39). The imaginary parts of the eigenangle which lead to modal attenuation can also be ignored when multiplied by $\bar{x}$ in the exponents of Eq.(39). Moreover, the real parts of the sines of the eigenangles are very nearly one and may be replaced by this value where they multiply $\bar{x}$ in Eq.(39). Using these conditions and the following spectrum relationship, $w(k_x, k_y)$, for the random surface,

$$2\pi w(k_x,k_y) = \iint_{-\infty}^{\infty} \rho(\bar{x},\bar{y})\exp(-jk_x\bar{x}-jk_y\bar{y})d\bar{x}d\bar{y}, \tag{40}$$

Eq.(39) transforms to

$$\frac{1}{2} < E_y^{(s)}H_z^{(s)*} > = -\frac{|B|\hat{c}}{2\eta} 2\pi w(2k,o)\iint_{-\infty}^{\infty} \frac{dXdY}{X^2} \sum_{mnpq}\sum\sum\sum$$

$$\cdot\left[C_mC_nC_p^*C_q^*\lambda_m\lambda_n\lambda_p^*\lambda_q^* \exp(-jk((S_m+S_n)X)-(S_p^*+S_q^*)X))e_{ym}(z_T)e_{yn}(z_T)e^*_{yp}(z_T)e^*_{yq}(z_T)\right]. \tag{41}$$

It will next be assumed that the field is sufficiently constant over the illuminated area so that

$$\int f(X)dX \simeq \Delta X f(X). \tag{42}$$

Where ΔX is the pulse length and X the range to the midpoint of the illuminated area. The final integral reduction of Eq.(41) is made by replacing dY by $Xd\phi$ and by assuming an azimuthal beam pattern of the form

$$G(\phi) = \exp(-\ell n(2)\ (\phi/\phi_o)^2), \tag{43}$$

where ϕ_o is the 3dB halfwidth in radians. With this replacement Eq.(41) reduces to

$$\frac{1}{2}\langle E_y^{(s)} H_y^{(s)*}\rangle = -\frac{|B|^2}{2\eta}\left(\frac{\pi}{\ell n2}\right)^{1/2} 2\pi\phi_o\ w(2k,o)\ \frac{\Delta X}{X}\ \Sigma\Sigma\Sigma\Sigma_{mnpq}$$

$$\cdot\left[C_m C_n C_p^* C_q^* \lambda_m \lambda_n \lambda_p^* \lambda_q^* \exp(-jk((S_m+S_n)X(S_p^*+S_q^*)X))e_{ym}(z_T)e_{yn}(z_T)e_{yp}^*(z_T)e_{yq}^*(z_T)\right]. \tag{44}$$

Equation (44) exhibits the following expected backscatter behavior

1. That the backscatter power flux is proportional to the power spectrum of the surface evaluated at the Bragg wavenumber.
2. An inverse falloff with distance.
3. Proportionality to pulse length and beamwidth.
4. Two way attenuation between transmitter location and scatterer.
5. Essentially a fourth power dependence on grazing angle. Recall that θ is the angle of incidence so that the grazing angle, γ, equals $\pi/2-\theta$ and that to good approximation $C_m = \sin\gamma_m \simeq \gamma_m$.

Though somewhat outdated, the wave height power spectrum $w_p(k)$ suggested by Pierson[9] is used in subsequent calculations. If σ is used for the rms surface height, w and w_p are related as follows

$$\sigma^2 = \frac{1}{2\pi} \iint_{-\infty}^{\infty} w(k_x,k_y)dk_x dk_y = \frac{1}{2\pi} \int_o^{\infty} kdk \int_o^{2\pi} w(k,\phi)d\phi = \int_o^{\infty} w_p(k)dk. \tag{45}$$

If $w(k,\phi) = w(k)g(\phi)$ with $g(\phi)$ defined such that

$$\frac{1}{2\pi} \int_o^{2\pi} g(\phi)d\phi = 1, \tag{46}$$

then

$$\int_o^{\infty} w(k)kdk = \int_o^{\infty} w_p(k)dk, \tag{47}$$

so that $w(k) = w_p(k)/k$. Equation (44) expressed in terms of the Pierson spectrum and in terms of grazing angles becomes

$$\frac{1}{2} < E_y^{(s)} H_y^{(s)*} > = - \frac{|B_1|^2}{2\eta} \left(\frac{\pi}{\ell\eta 2}\right)^{1/2} 2\pi\phi_o \left[\frac{w_p(2k)}{2k}\right] \frac{\Delta X}{X} \sum\sum\sum\sum_{mnpq}$$

$$\cdot \left[\gamma_m\gamma_n\gamma_p^*\gamma_q^*\lambda_n\lambda_m\lambda_p^*\lambda_q^* \exp(-jk((\cos\gamma_m+\cos\gamma_n)\ X - (\cos\gamma_p^*+\cos\gamma_q^*)X))\right.$$

$$\left. \cdot\ e_{ym}(z_T)e_{yn}(z_T)e_{yp}^*(z_T)e_{yq}^*(z_T)\right]. \tag{49}$$

For purposes of path loss calculations presented subsequently, Equation (49) is multiplied by the effective receiver area π/k^2 and divided by the antenna gain, 3/2, times the free space power radiated by the dipole. That is Equation (49) is to be multiplied by the factor,

$$\frac{\pi}{k^2} \frac{2}{3} \frac{3\eta}{4\pi k^4} \left(\frac{4\pi\epsilon_o}{p}\right)^2.$$

Multiplying Eq.(49) by this factor, discarding the negative sign which simply signifies energy propagating in the negative x direction and expressing the result as path loss in dB gives

$$PL(dB) = -10\ \mathrm{Log}_{10}\left\{2.581\times10^{6}\ f_{gh}^{4}\ \phi_o\left[\frac{w_p(2k)}{2k}\right]\frac{\Delta X}{X}\sum\sum\sum\sum_{mnpq}\right.$$

$$\cdot\left[\gamma_m\gamma_n\gamma_p^*\gamma_q^*\lambda_n\lambda_m\lambda_p^*\ \lambda_q^*\ \exp\left(-jk\left[(\cos\gamma_m+\cos\gamma_n)X\ -\ (\cos\gamma_p^*+\cos\gamma_q^*)X\right)\right]\right]$$

$$\left.\cdot\ e_{ym}(z_T)\ e_{yn}(z_T)\ e_{yp}^*(z_T)e_{yq}^*(z_T)\right\}, \qquad (50)$$

where the frequency, f_{gh}, is to be expressed in gigahertz, the beamwidth ϕ_o in radians, and all other quantities in MKS units.

3.0 GRAVITY WAVE EFFECTS

The gravity wave or long wavelength region of the ocean surface spectrum has several effects which are generally allowed for in very approximate fashion. The first of these which will be discussed is the effect on the forward propagating wave. In this study this effect is approximated by simply modifying as follows the ground reflection coefficient used for the waveguide calculations[2,3]

$$(\bar{R}_{\perp m})_R = (\bar{R}_{\perp m})_F\ \exp(-2(k\delta)^2\ (n^2(o)-\beta_m^2)),\ \mathrm{Re}(n^2(o)-\beta_m^2) \geq 0$$

$$= (\bar{R}_{\perp m})_F,\ \mathrm{Re}(n^2(o)\ -\beta_m^2) < 0. \qquad (51)$$

Here the subscript R on $\bar{R}_\perp$ signifies the rough surface value whereas the subscript F signifies the flat earth value. Also, δ is the rms surface height, $n^2(o)$ is the square of the modified refractive index at the ground and β_m is the modal propagation constant divided by wavenumber. For $n^2(o) = 1$, the quantity $n^2(o) - \beta_m^2 = \sin^2\gamma_m$ where γ is the plane wave grazing angle at the surface and so the exponent in the term in that limit reduces to the well known factor $1/2\ \Phi^2$ with Φ the Rayleigh roughness parameter. The rms surface height used in subsequent calculation has been determined from the expression

$$\delta^2 = \int_o^{.359} w_p(k)dk, \tag{52}$$

by numerical integration. As will be shown later, this gives values which agree quite well with the often used formula $\delta \simeq .0051u^2$, where u is windspeed in m/s.

The composite-roughness theory of sea surface backscatter under free space conditions and within the line of sight makes allowance for grazing angles of incidence by introducing a shadowing function, $G(\gamma)$, and by allowing for tilting of the large scale surface. Discussing the first of these, the shadowing concept is taken over in the present study by simply multiplying Eq.(50) by $G(\gamma_{ro})$ where the subscript r pertains to the real part of the grazing angle and the subscript 0 pertains to the least attenuated mode. Using the real part of the eigenangle certainly seems to be a reasonable generalization for ducting environments for which $\gamma_r >> \gamma_i$ (subscript i for imaginary part). For standard or near standard propagation conditions the assumption becomes quite suspect since then $\gamma_i \geq \gamma_r$. Nevertheless, for lack of a rigorous prescription the assumption has been used for all cases in the subsequent calculations. Also, it is clear that it would be preferable to multiply each term in the quadruple sum which appears in Eq.(50) by an appropriate bistatic

shadowing function. However, since the eigenspace is quite densely packed the above procedure seems adequate especially in view of large uncertainties associated with the wave height spectrum. The shadowing function used is that given by Wagner[9]

$$G(\gamma_{ro}) = \frac{(1 + \mathrm{erf}(v))\ (1-\exp(2B))}{4B}, \tag{53}$$

where

$$v = \gamma_{ro}/(2\zeta^2)^{1/2}, \tag{54}$$

$$B = (\exp(-v^2) - \sqrt{\pi}\ \mathrm{verfc}(v))/(4\sqrt{\pi}v), \tag{55}$$

$$\mathrm{erf}(x) = \frac{2}{\sqrt{\pi}} \int_o^x \exp(-t^2)dt = 1 - \mathrm{erfc}(x). \tag{56}$$

Also, ζ in Eq. (54) is the rms slope of the large scale surface. Using formulas given by Chan and Fung[10], the upwind slope variance, ζ_u^2, and crosswind slope variance, ζ_c^2, are given by

$$\zeta_u^2 = \frac{1}{2}\ (1+\frac{1-\beta}{1+\beta}) \int_o^{.359} k^2\ w_p(k)dk, \tag{57}$$

$$\zeta_c^2 = \frac{1}{2}\ (1-\frac{1-\beta}{1+\beta}) \int_o^{.359} k^2\ w_p(k)dk. \tag{58}$$

The upper limit on the integrals should be frequency dependent. However, Chan and Fung have had moderate success for their line of sight cross section calculations using the value 0.359 and it has therefore been used in the present calculations. The quantity β is given by

$$\beta = \frac{\zeta_c^2}{\zeta_u^2} = \frac{.003+1.92\text{x}10^{-3}\ U_{12.5}}{3.16\text{x}10^{-3}\ U_{12.5}}. \tag{59}$$

Where $U_{12.5}$ is the wind speed in meters/sec at an altitude of 12.5 m. Equation (59) was given by Cox and Munk.[11] The results given in the following section presume wind speeds at 19.5 m. To calculate β for a given wind speed in m/s at 12.5 m the so called frictional velocity, u_f, is first calculated by iteration from the equations[12]

$$10^2 U_{19.5} = \frac{u_f}{.4}\, \ell\eta \left(\frac{1950}{z_o}\right), \tag{60}$$

$$z_o = .684/u_f + 4.28\text{x}10^{-5}u_f^2 - 4.43\text{x}10^{-2}. \tag{61}$$

with the friction velocity determined, $U_{12.5}$ in m/s is found from the equation

$$10^2\ U_{12.5} = \frac{u_f}{.4}\, \ell\eta\ (\frac{1250}{z_o}). \tag{62}$$

Using this value in Eq.(59) gives β which in turn enables the calculation of ζ_c^2 and ζ_u^2 as well as the corresponding shadow function (53). Results given in the following section presume upwind conditions.

Approximate allowance for tilting caused by the large scale surface roughness is made by simply noting that if the slope of the large scale surface is η, then the grazing angle becomes $\gamma + \eta$. With this replacement, each term of the quadruple sum in Eq.(50) should be averaged over the illuminated portion of the surface. However, the eigenangles are on the order of several milliradians whereas $\left(\overline{\eta^2}\right)_{i\ell}^{1/2}$ is on the order of tenths of radians. Here the bar denotes averaging and the subscript $i\ell$ denotes that the averaging is to be

taken over the illuminated portion of the surface. Because $\left(\overline{\eta 2}\right)_{i\ell}^{1/2} >> |\gamma_m|$, the principal term in the quadruple product is the one which varies as $\left(\overline{\eta 4}\right)_{i\ell}$. Thus, as a simplifying assumption each of the grazing angles in Eq.(50) is replaced by $\gamma + \left(\overline{\eta 4}\right)_{i\ell}^{1/4}$. This allows for the path loss to be written as

$$PL(dB) = -20\ Log_{10}\Big[1.607x10^3 f_{gh}^2 \left(\phi_o \frac{w_p(2k)}{2k} \frac{\Delta X}{X} G(\gamma_{ro})\right)^{1/2} \Big| \sum_{mn}\sum$$

$$\cdot (\gamma_m + \left(\overline{\eta 4}\right)_{i\ell}^{1/4})(\gamma_n + \left(\overline{\eta 4}\right)_{i\ell}^{1/4}) \exp(-jk((\cos\gamma_n + \cos\gamma_m)X)) e_{ym}(z_T) e_{yn}(zt) \Big| \Big], \qquad (63)$$

where the vertical lines, $||$, denote absolute values.

Slope averaging over the illuminated surface has been discussed by Wagner[9] and McDaniel[13]. The grazing angles dealt with here are sufficiently small that the averaging equation may be written as

$$\left(\overline{\eta^4}\right)_{i\ell} \simeq \frac{2}{\sqrt{2\pi\zeta^2}} \int_o^\infty \eta^4 \exp(-\eta^2/2\zeta^2) d\eta = 3\zeta^4, \qquad (64)$$

where ζ is the rms slope of the large scale surface previously discussed in connection with Eq.(54). For the purpose of the calculations given in the following section, ζ^2 has been calculated using the upwind formula given by Eq.(57).

4.0 RESULTS

Tappert has given backscatter results for a single surface realization for the standard atmosphere and for two evaporation ducts. The latter are characterized by duct heights of 14 and 28 m and have been described by Hitney.[14] Tappert's calculations are for a frequency of 9.6 GHz, a transmitter height of 25 m, a pulse width of 0.5 μs (in our convention $\Delta X = cT$ with c the speed of light and T pulse width), and a 3 dB full beam width of 1.2°. In this section waveguide backscatter results based on Eq.(63) will be compared with Tappert's results. Tables 1 and 2 below give the constituents of Eq.(63) calculated from the Pierson spectrum and the shadowing function calculated using Wagner's formula. The method of calculation has been described in the previous section.

Table 1. Wave spectrum related quantities.

Wind Speed (kts)	$\sqrt{\delta}$ (m)	ς^2	$(\overline{\eta^4})i\ell$	$w_p(2k)/2k$ (m^4)
10	.141	.0103	3.18e-4	6.26e-13
20	.565	.0186	1.04e-3	1.63e-12
30	1.277	.0306	2.81e-3	3.09e-12
40	2.272	.0444	5.91e-3	4.85e-12

Table 2. Shadow function.

Wind Speed (kts)	$G(\gamma_{ro})$		
	STD ATMOS	14m Duct	28m Duct
10	1.01e-2	6.45e-2	9.91e-2
20	1.01e-2	4.68e-2	7.14e-2
30	1.01e-2	3.60e-2	5.45e-2
40	1.01e-2	2.95e-2	4.47e-2

The quantities in table 1 which depend upon integration of the Pierson spectrum have been numerically integrated using a Romberg integration scheme with a self adjusting step size. Tabular values of the rms bump height will be seen to agree quite well with the often used formula $\sigma \approx .0051u^2$ with u in m/s. Values of ς^2 given in table 1 agree quite well with values interpolated from tabulations given by Chan and Fung. For the standard atmosphere the shadow function is independent of wind speed. The reason for this is that the lowest attenuated mode (indeed all modes calculated for this case) is evanescent at the ground and so the rms height correction to the ground reflection coefficient does not apply.

Figures 1, 2, and 3 show path loss as a function of range for the standard atmosphere, the 14 m duct and the 28 m duct in that order. Each plot shows results for wind speeds of 10, 20, 30 and 40 knots. The arrow on the horizontal axis shows the normal horizon.* Thus, a sufficient number of modes have been used for the calculations to allow for the waveguide fields to be carried well within the normal horizon. All modes with attenuation rates less than 20 dB/km were used for the standard atmosphere calculations and all modes with attenuation rates less than 2.1 dB/km were used for the evaporation duct calculations. In particular, 24 modes were used for the standard atmosphere calculation; between 82 and 97 modes, depending upon windspeed, were used for the 14 m duct calculations and between 94 and 109 modes were used for the 28 m duct calculations. For ranges beyond and comparable to the normal horizon probably 2 or 3 modes at the most would have been sufficient for the propagation geometry considered. Figures 1 through 3 show that the mode sums break down for the 25 m transmitter height at ranges between about 4 and 9 km. Curves for the standard atmosphere, the 14 m duct and the 28 m duct all show a tendency towards saturation as the wind speed increases. Because of field evanescence at the ground, application of shadowing concepts is particulary

* For the geometry considered, the extended radio horizon for the 14 m duct is about 56 km and about 81 km for the 28 m duct.

questionable in the case of the standard atmosphere. In the absence of allowance for shadowing, the path loss in this instance would be reduced by about 20dB (see table 2).

Figures 4 through 15 show comparisons with Tappert's single surface realization calculations. To produce the comparisons, the path loss has been subtracted from the 160 dB system gain (40 dB transmitter gain, 40 dB receiver gain and 80 dB transmitted power). In addition to average signal levels, the parabolic equation results give some measure of fluctuation about the average field. This presumably results from the features of the illuminated surface varying with range. To estimate rms fluctuations with waveguide formalism would require carrying the scatter calculation to higher order. No attempt has been made to do that. Figures 4 through 15 show that the average field fall off (attenuation rate) as determined by the parabolic equation and waveguide formalism are similar.

To give an idea of the magnitude of the difference between the average field as determined by the two methods, table 3 gives the difference at 20 km (the average field determined by the parabolic equation calculation has been determined by subjectively drawing a curve through the center of the fluctuating signal).

Table 3. Comparison of average fields at 20 km.

Wind Speed (kts)	$[E_{ywg} - \bar{E}_{ype}]$(dB)		
	STD Atmosphere	14 m Duct	28m Duct
10	+ 11.4	- 2.3	- 8.0
20	+ 6.0	- 8.0	- 4.6
30	+ 8.8	0.0	- 7.1
40	+ 11.1	0.0	0.0

The subscripts WG and PE in table 3 denote waveguide and parabolic equation results respectively. The bar over E_{ype} denotes the subjective average mentioned above. The largest discrepancies occur for the standard atmosphere with the waveguide results consistently higher than the parabolic equation results. The most favorable comparison is for the 14 m duct where there is essentially no difference for the 30 and 40 knot wind speed cases. In contrast to the standard atmosphere comparisons the waveguide values are less than the parabolic equation results for the 14m and 28m evaporation ducts.

No attempt has been made to use the same wave height power spectrum used by Tappert; but, rather, in this initial effort the decision was made to use the Pierson spectrum which has been used by Chan and Fung, and McDaniel with modest success at more oblique incidence. Of lesser importance is the fact that Tappert's results are for an infinitely conducting ground, whereas the present calculations are for a seawater conductivity of 21 Si/m and a seawater dielectric constant of 54.3. In view of the approximate allowance for surface roughness on forward propagation, the non-rigorous introduction of shadowing and tilting concepts along with the omission of multiple scatter effects, the agreement exhibited by figures 4 through 15 and table 3 is very much better than expected.

5.0 DISCUSSION

Generally, normal mode methods have been used to assess the adequacy of parabolic equation solvers for propagation in either acoustic or electromagnetic channels. Recent results by Tappert, using parabolic equation and Monte Carlo methods, for electromagnetic backscatter in evaporation ducts afford an opportunity to use parabolic equation results to assess the adequacy of using waveguide methods for treating backscatter for very grazing angles (i.e. modal angles on the order of several milliradians). In particular, the parabolic

equation results allow for an assessment of classical approximations used to treat long surface wavelength effects. These include applicability of Kirchhoff theory for forward propagation along with shadowing and tilting of the local surface. In this study, results at 9.6 GHz have been generated based on first order Bragg scatter in a waveguide environment coupled with the long surface wavelength effects just mentioned. Comparisons of the results with Tappert's single surface realization are shown in figures 4 through 15. Those comparisons show very similar attenuation rate behavior for the ducting environments considered (i.e. normal atmosphere, 14 and 28 m evaporation ducts with 10, 20, 30, and 40 knot wind speeds). Average levels compare to within about ± 10 dB (see table 3). Some of this difference is probably due to the fact that Pierson's surface height spectrum has been used in the present study whereas Tappert used yet another spectrum. Nevertheless, in view of the crude and certainly questionable methods for treating long wavelength effects, the comparisons are surprisingly good and, at the very least, intriguingly curious. Certainly, additional comparisons should be made.

The object of this study has been to explore the possibility of using waveguide concepts for backscatter calculations and not the development of a general purpose computer program. Thus, surface quantities such as rms bump height, tilting angle, shadowing function, etc. have been calculated using routines separate from the waveguide program. An automated program requires the merging of these programs. Formulas for line of sight backscatter for horizontally stratified environments should be developed and added to the program. This would allow scatter calculations for ranges less than ≈ 8 km where the mode sums break down in the present case studies. Only horizontal polarization has been treated. Expectations are that vertical polarization would behave in similar fashion beyond the horizon. Within the line of sight, however, differences are likely and results applicable to vertical polarization should be developed. Lastly, first order scatter results were used in

the present study. To estimate variances of the scattered fields higher order results are required. That would be a challenging and interesting extension of the present study.

References

1. Ulaby, F.T., R.K. Moore and A.K. Fung. 1982. *Microwave Remote Sensing Active and Passive, Vol. II: Radar Remote Sensing and Surface Scattering and Emission Theory*, Addison-Wesley Publishing Co., London.

2. Ament, W.D. 1953. "Toward a Theory of Reflection by a Rough Surface", *Proc. IRE*, vol. 41, pp. 142-146.

3. Beckmann, P. and H. Spizzichino. 1963. *The Scattering of Electromagnetic Waves from Rough Surfaces*, Pergamon and MacMillan, New York.

4. Fung, A.K. and H.L. Chan. 1969. "Backscattering of Waves by Composite Rough Surfaces", *IEEE Trans. Antennas & Propagation*, AP-17, pp. 590-597.

5. Peake, W.H., D.L. Barrick, A.K. Fung and H.L. Chan. 1970. Comments on "Backscattering of Waves by Composite Rough Surface," *IEEE Trans. Antennas & Propagation*, AP-18, pp. 716-728.

6. Bass, F.G. and I.M. Fuks. 1979. *Wave Scattering From Statistically Rough Surfaces*. Pergamon Press, New York.

7. Pappert, R.A. 1968. "On the Problem of Horizontal Dipole Excitation of the Earth-ionosphere Waveguide", TR 684 (Mar). Naval Electronics Laboratory Center (now NOSC), San Diego, CA.

8. Pierson, W.J. 1976. "The Theory and Applications of Ocean Wave Measuring Systems at and Below Sea Surface on the Land, From Aircraft and From

Spacecraft", NASA CR-2646. Naval Aeronautic and Space Administration, Washington, DC.

9. Wagner, R.J. 1967. "Shadowing of Randomly Rough Surfaces", *Jour. Acous. Soc. Amer.*, vol. 41, no. 1, pp. 138-147.

10. Chan, H.L. and A.K. Fung. 1977. "A Theory of Sea Scatter at Large Incidence Angles", *Jour. Geophys. Res.*, vol. 82, no. 24, pp. 3439-3444.

11. Cox, C. and W. Munk. 1954. "Measurement of the Roughness of the Sea Surface from Photographs of the Sun Glitter", *Jour. Opt. Soc. Amer.* 44(11), 838-850.

12. Pierson, W.J. and R.A. Stacy. 1973. "The Elevation, Slope and Curvature Spectrum of a Wind Roughened Sea Surface, NASA CR-2247, Naval Aeronautic and Space Administration, Washington, DC.

13. McDaniel, S.T. and A.D. Gorman. 1982. "Acoustic and Radar Sea Surface Backscatter", *Jour. Geophys. Res.*, vol. 87, no. C6, pp. 4127-4136.

14. Hitney, H.V. 1988. "Evaporation Duct Effects on Low Altitude Propagation: Guidelines for the NATO AAW Systems Project, NOSC TR 1304 (Jun). Naval Ocean Systems Center, San Diego, CA.

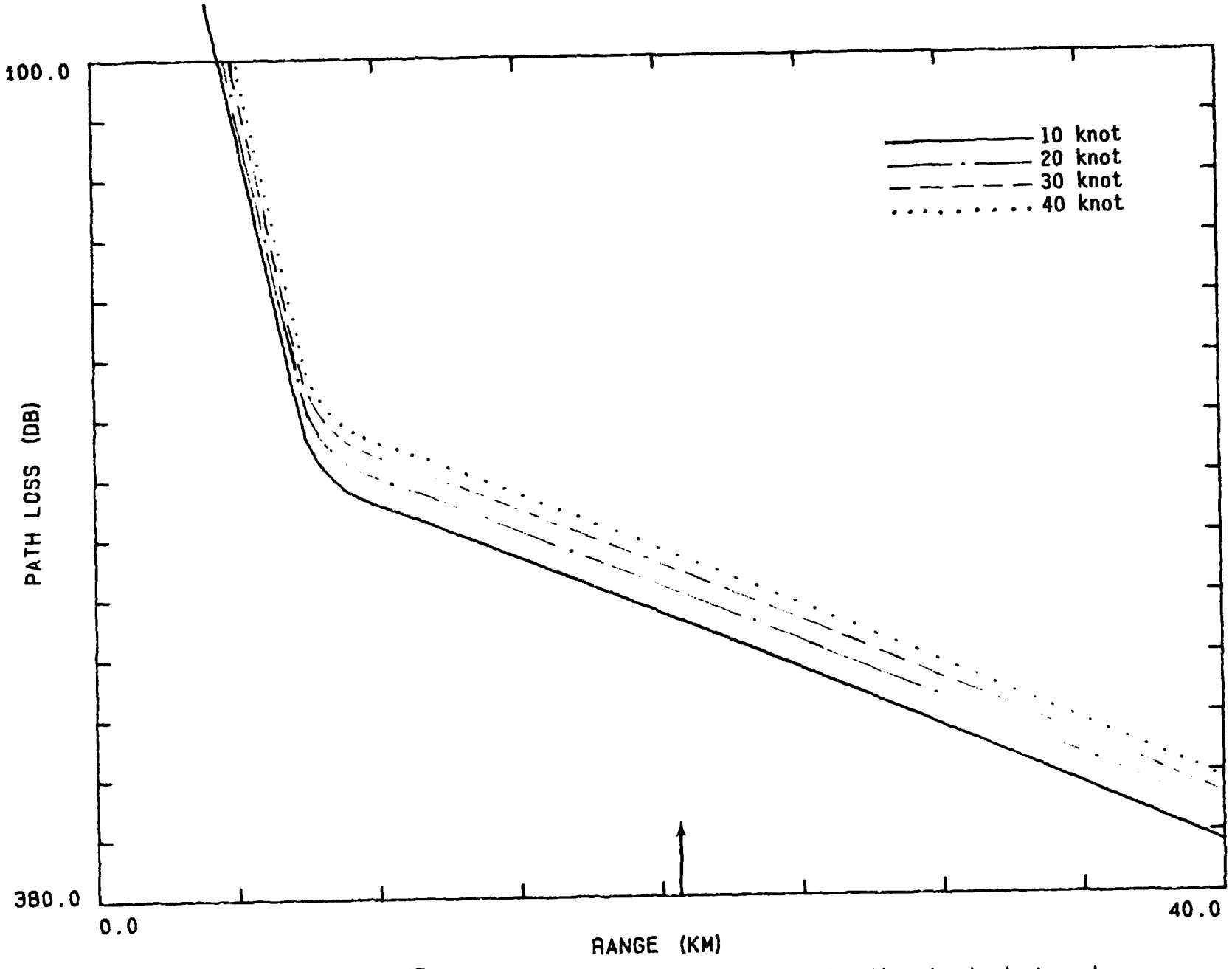

Figure 1. Path loss vs. range for the standard atmosphere. Transmitter-receiver height 25m.

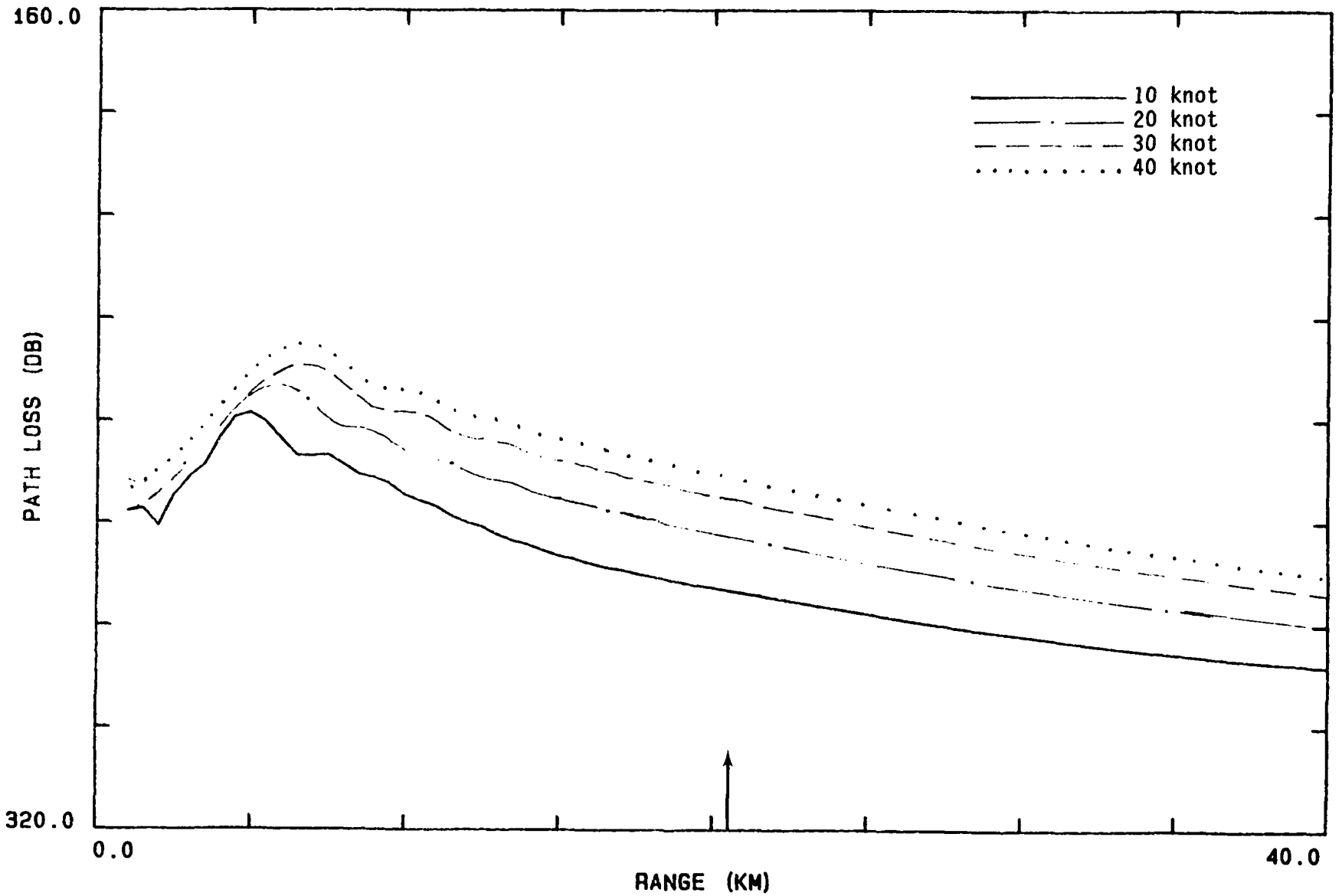

Figure 2. Path loss vs. range for a 14m evaporation duct. Transmitter-receiver height 25m.

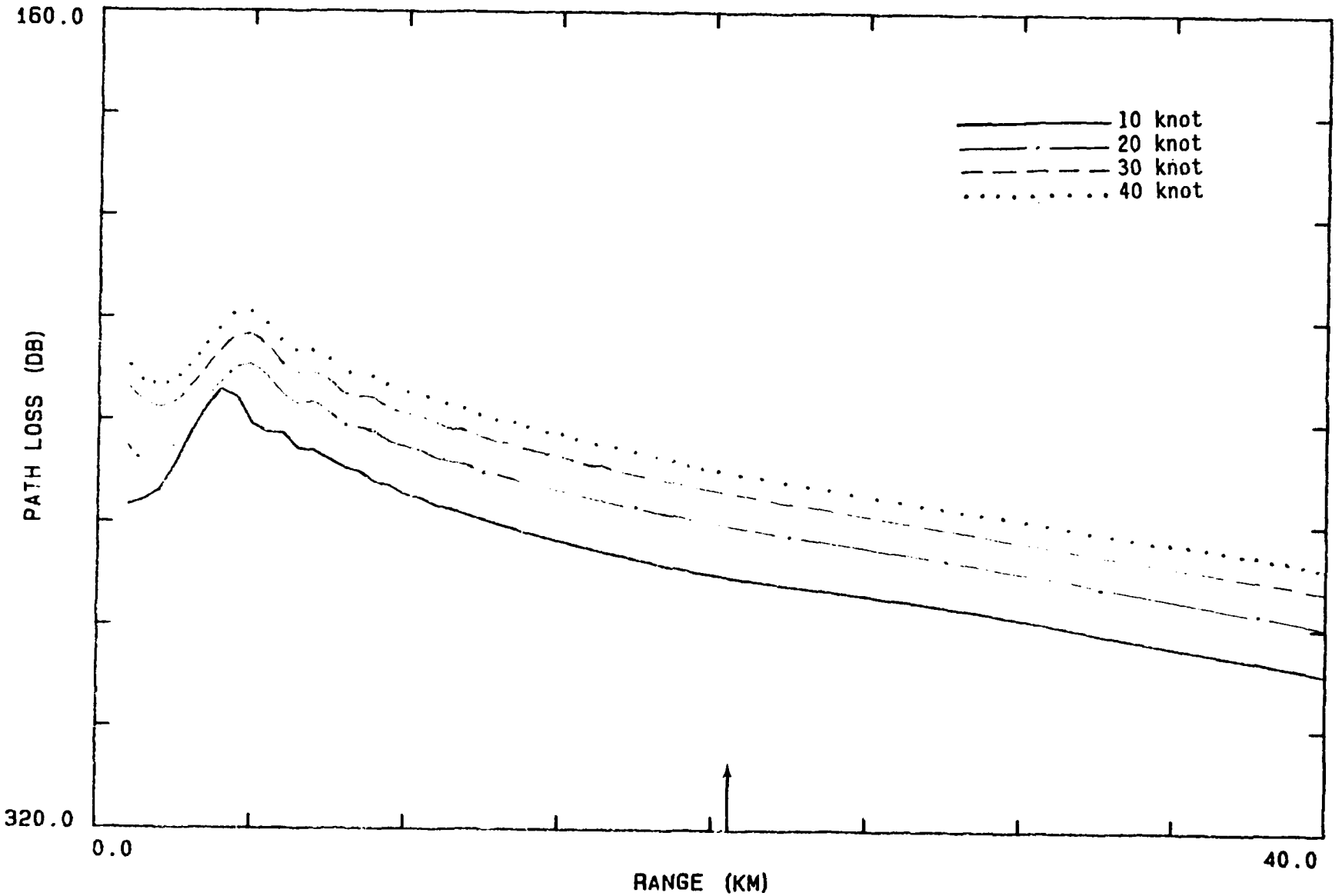

Figure 3. Path loss vs. range for a 28m evaporation duct. Transmitter-receiver height 25m.

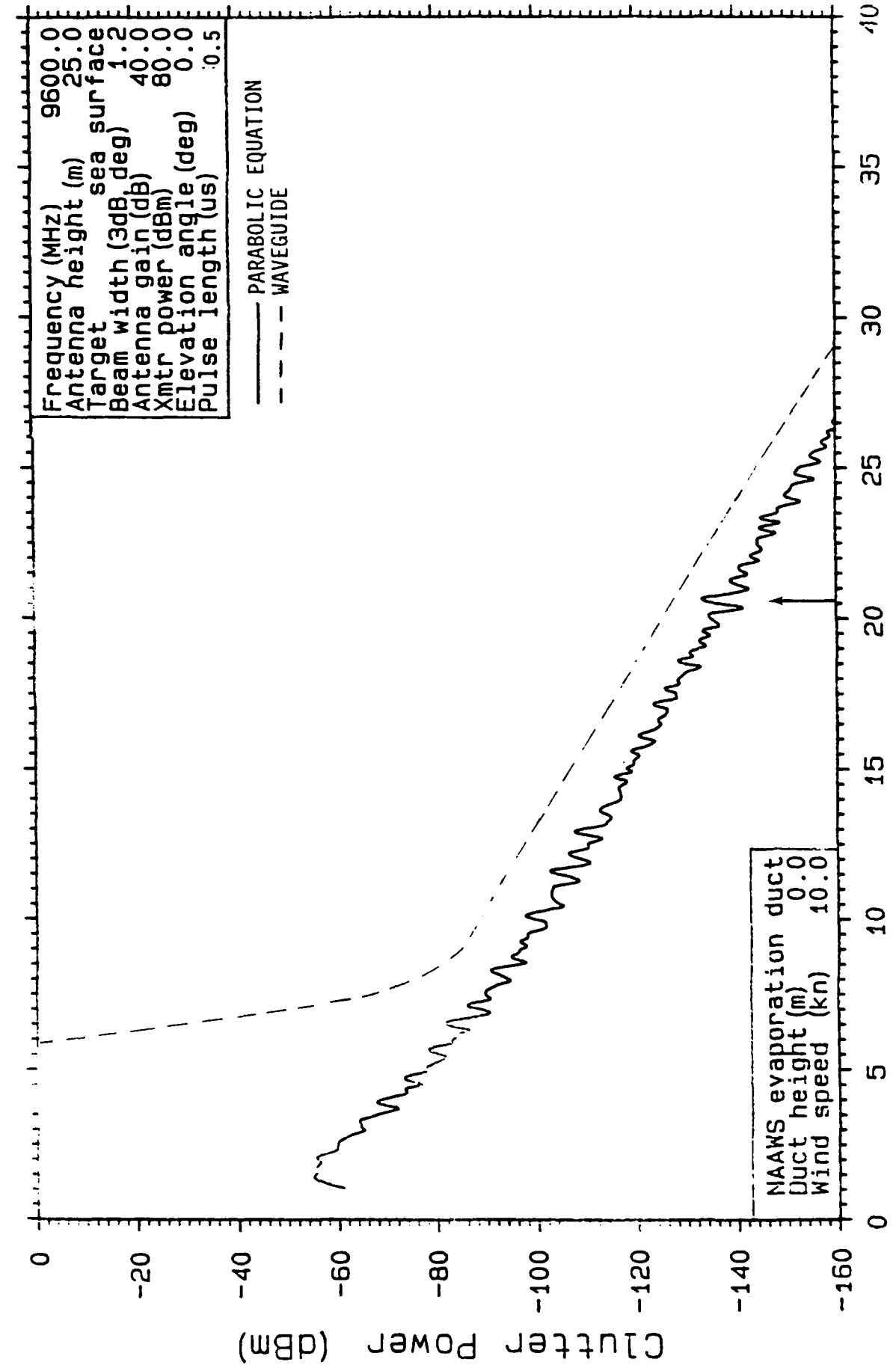

Figure 4. Clutter power vs. range. Comparison between pe and waveguide results. Standard atmosphere, 10 knot wind.

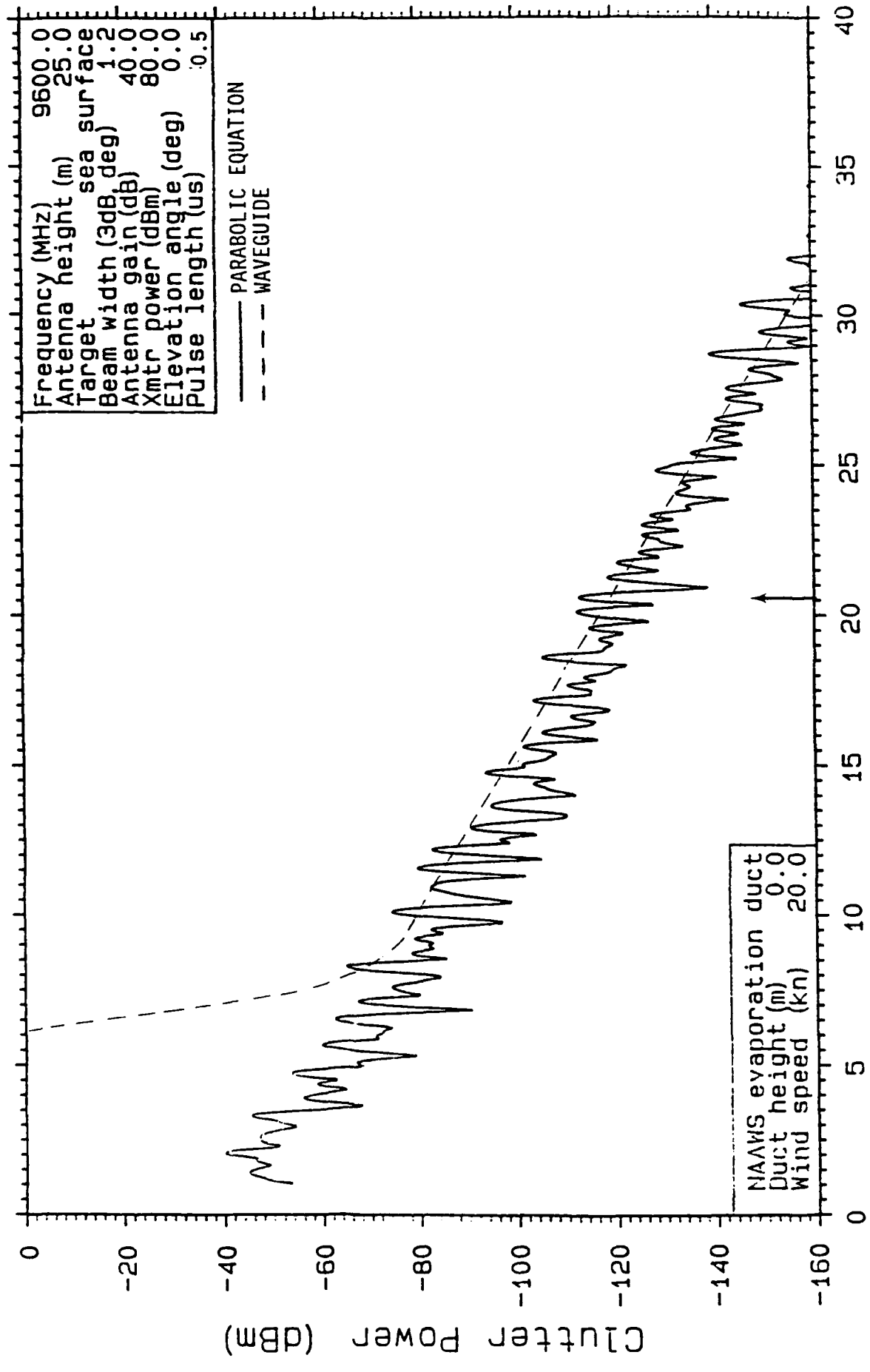

Figure 5. Clutter power vs. range. Comparison between pe and waveguide results. Standard atmosphere, 20 knot wind.

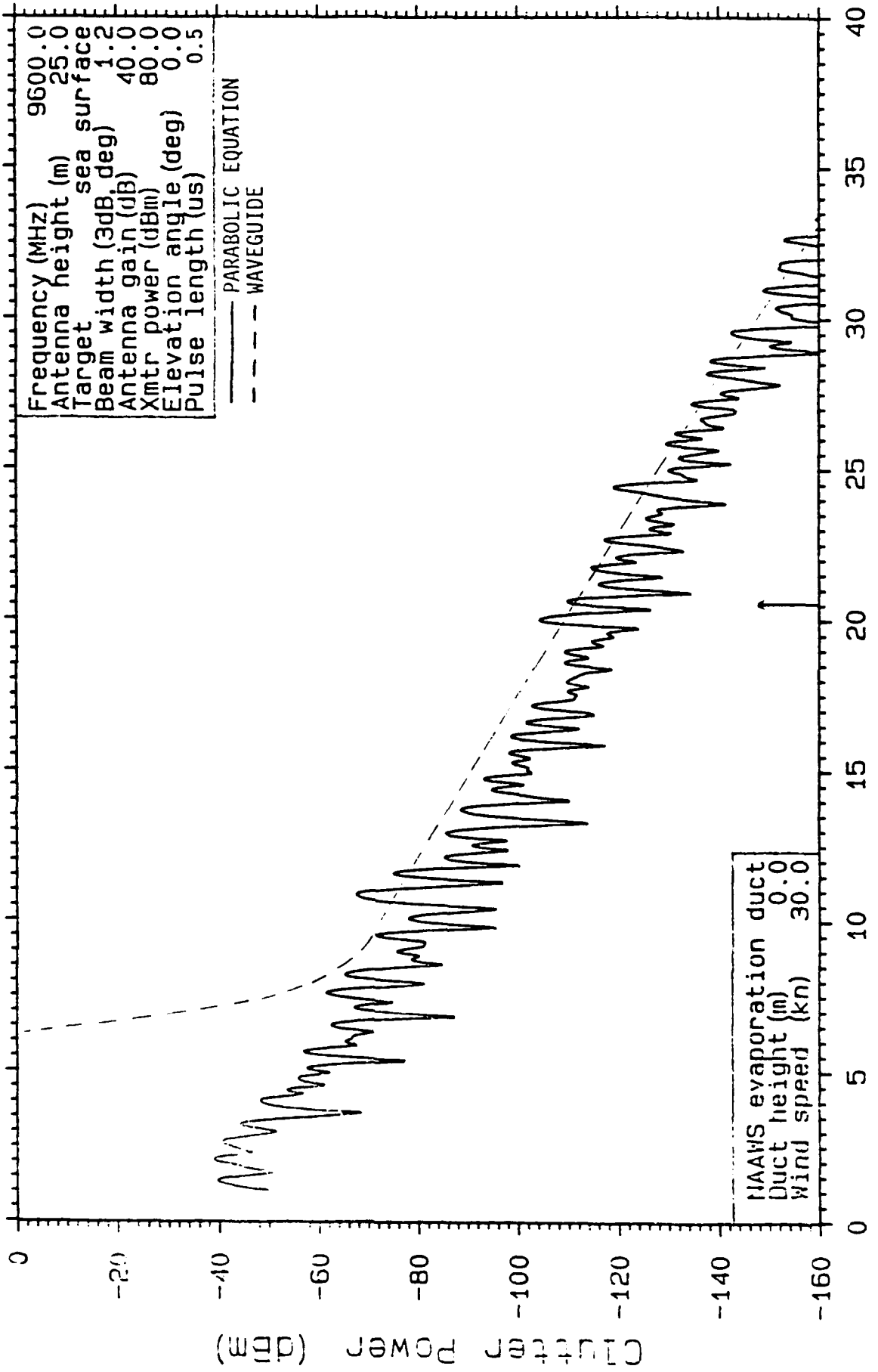

Figure 6. Clutter power vs. range. Comparison between pe and waveguide results. Standard atmosphere, 30 knot wind.

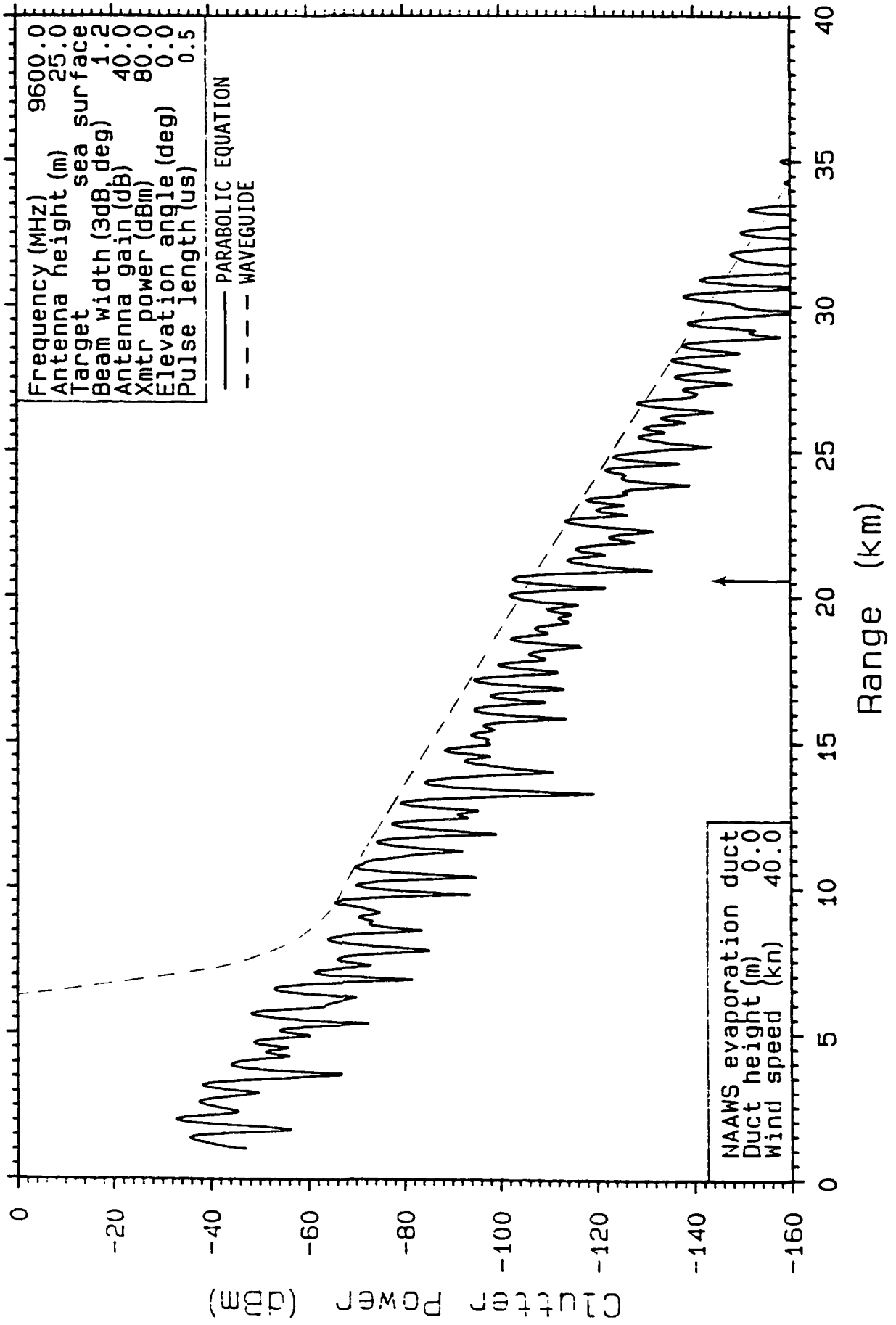

Figure 7. Clutter power vs. range. Comparison between pe and waveguide results. Standard atmosphere, 40 knot wind.

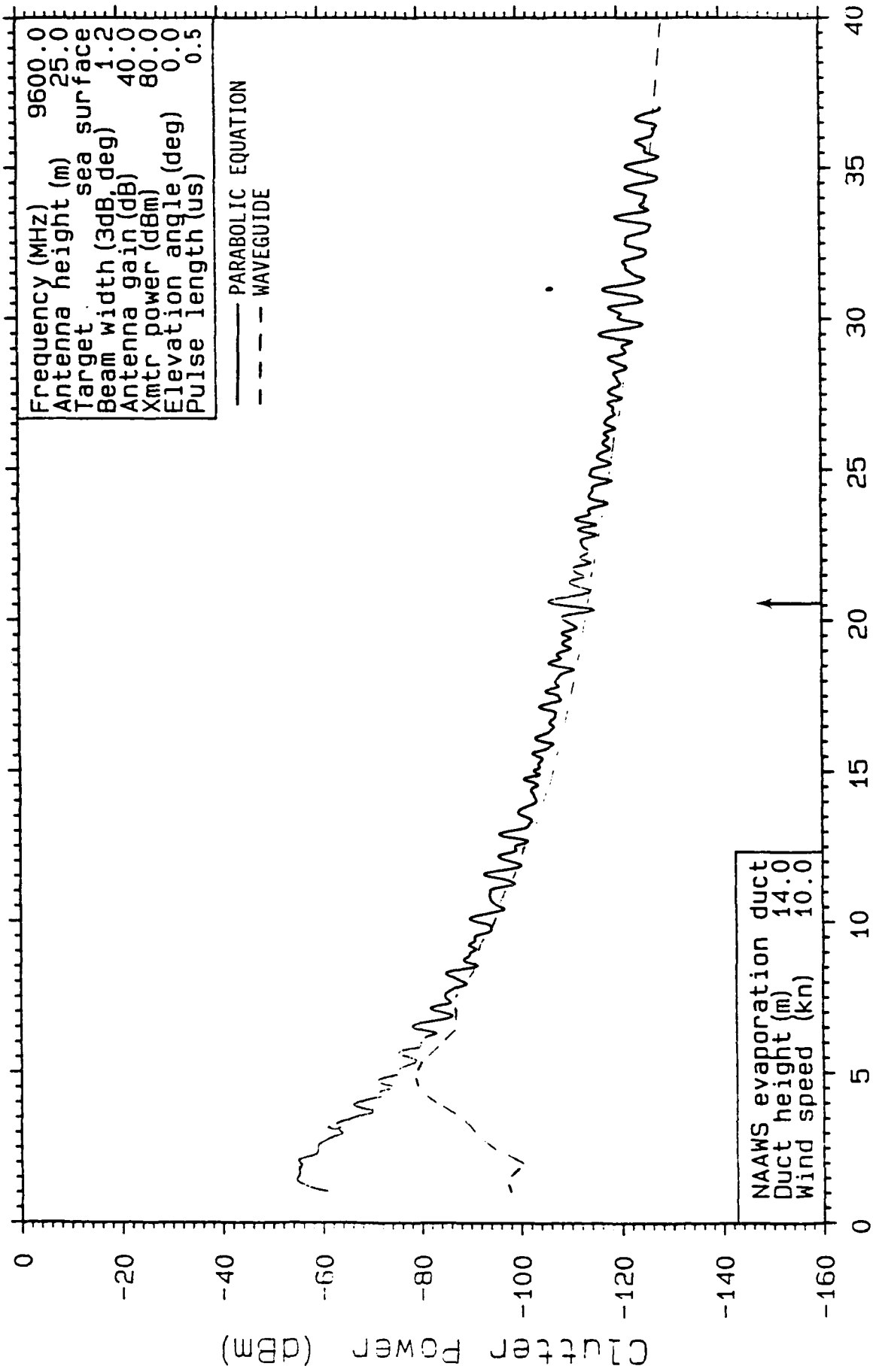

Figure 8. Clutter power vs. range. Comparison between pe and waveguide results. Fourteen meter evaporation duct, 10 knot wind.

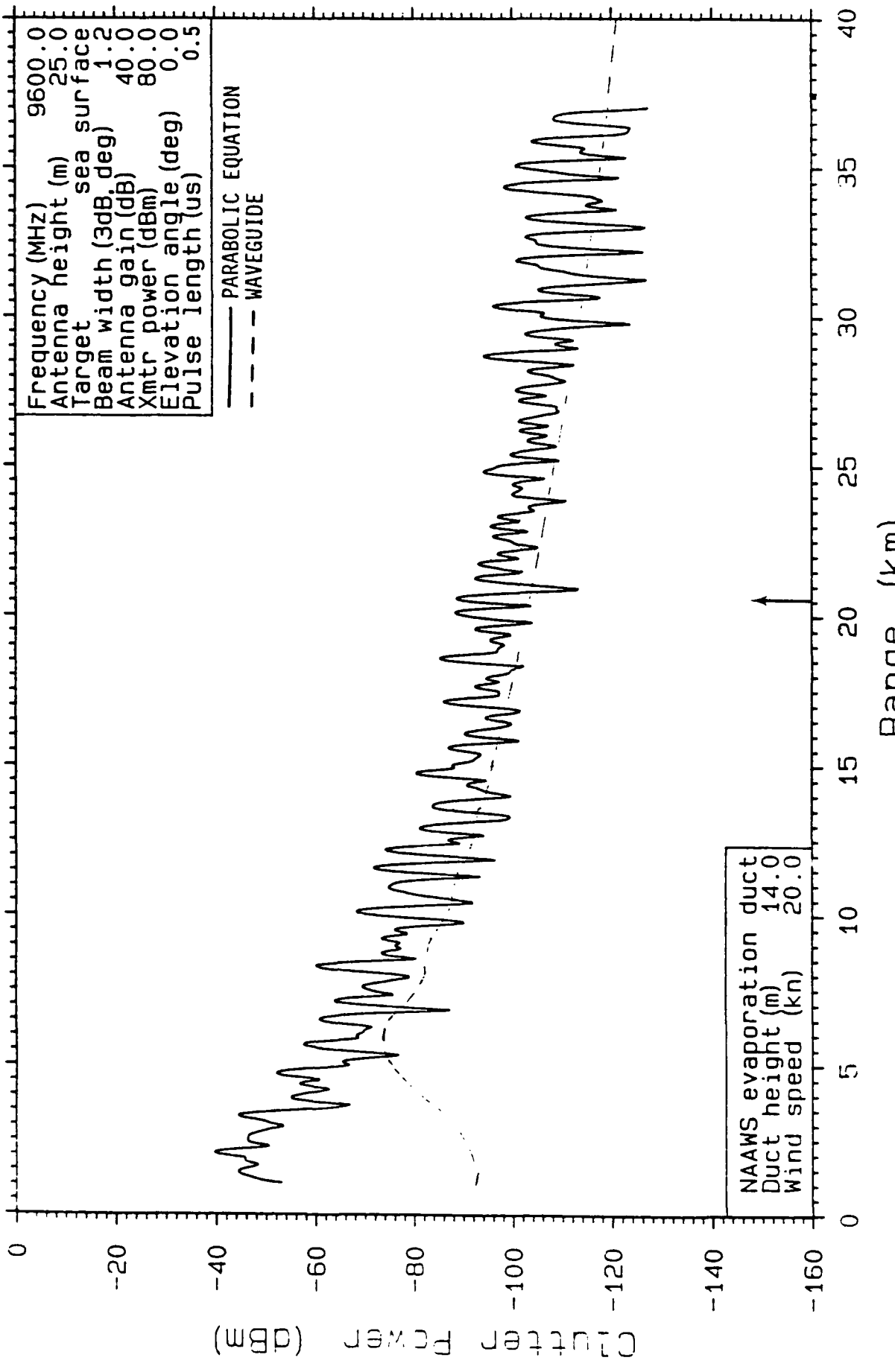

Figure 9. Clutter power vs. range. Comparison between pe and waveguide results. Fourteen meter evaporation duct, 20 knot wind.

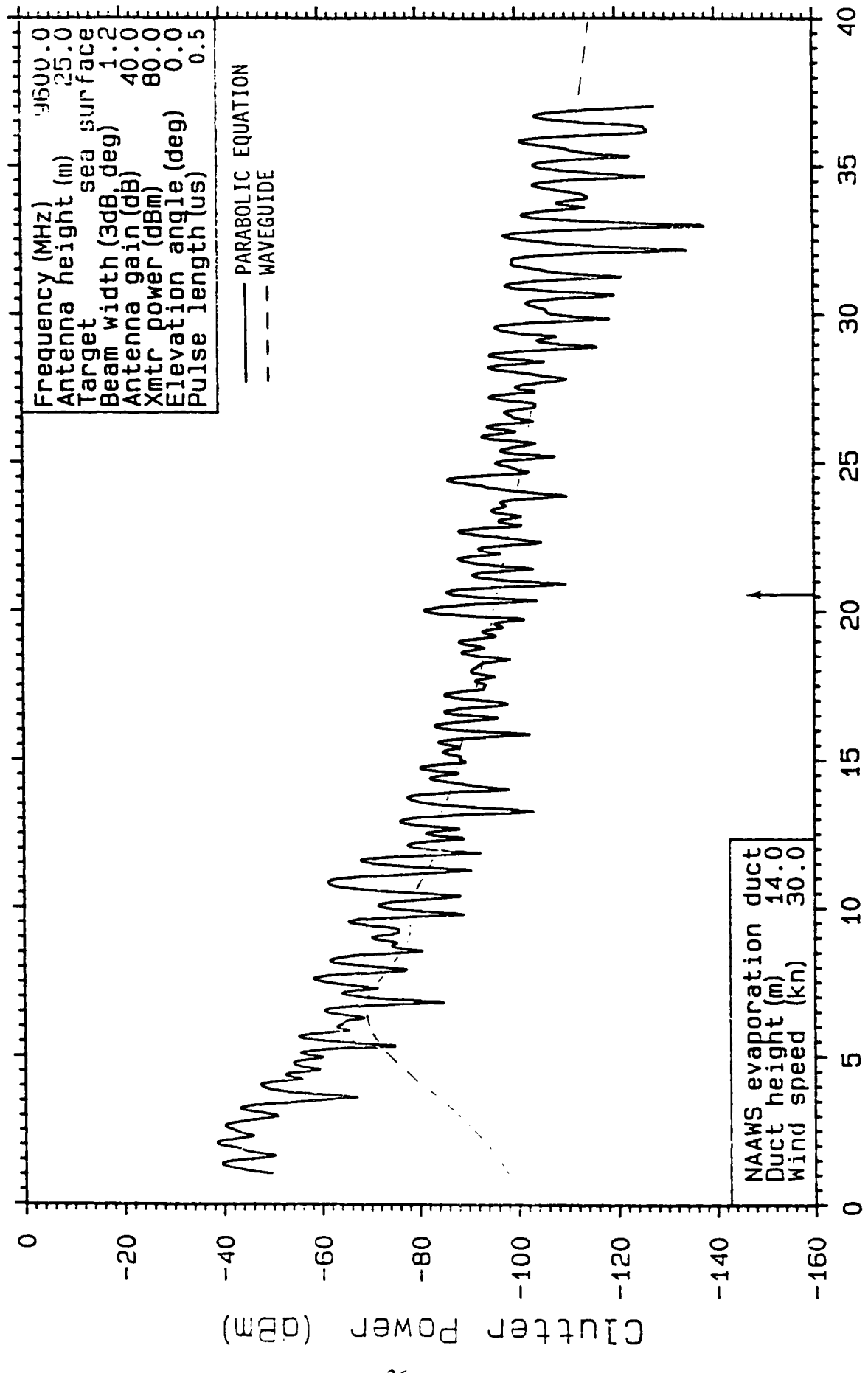

Figure 10. Clutter power vs. range. Comparison between pe and waveguide results. Fourteen meter evaporation duct, 30 knot wind.

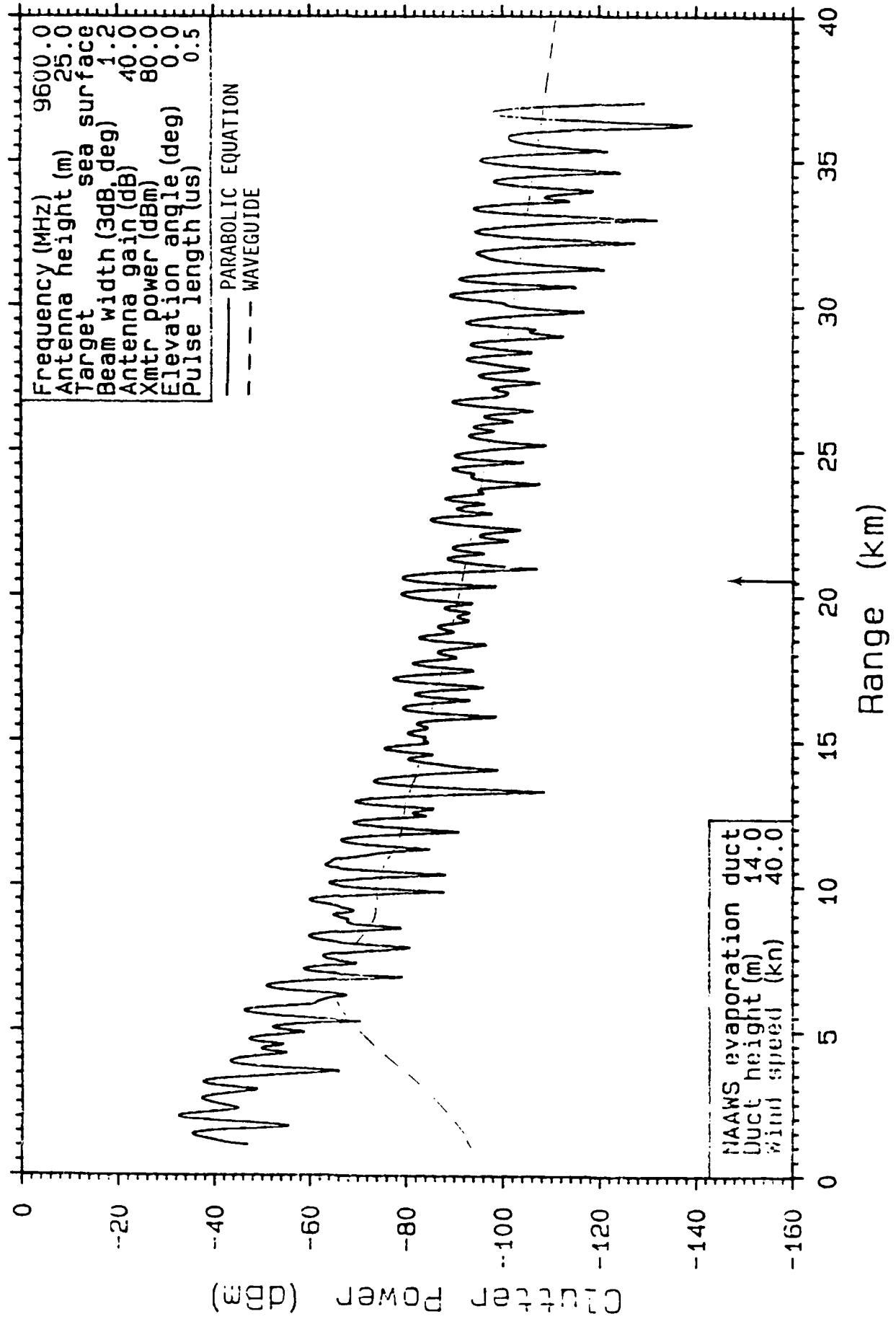

Figure 11. Clutter power vs. range. Comparison between pe and waveguide results. Fourteen meter evaporation duct, 40 knot wind.

Figure 12. Clutter power vs. range. Comparison between pe and waveguide results. Twenty eight meter evaporation duct, 10 knot wind.

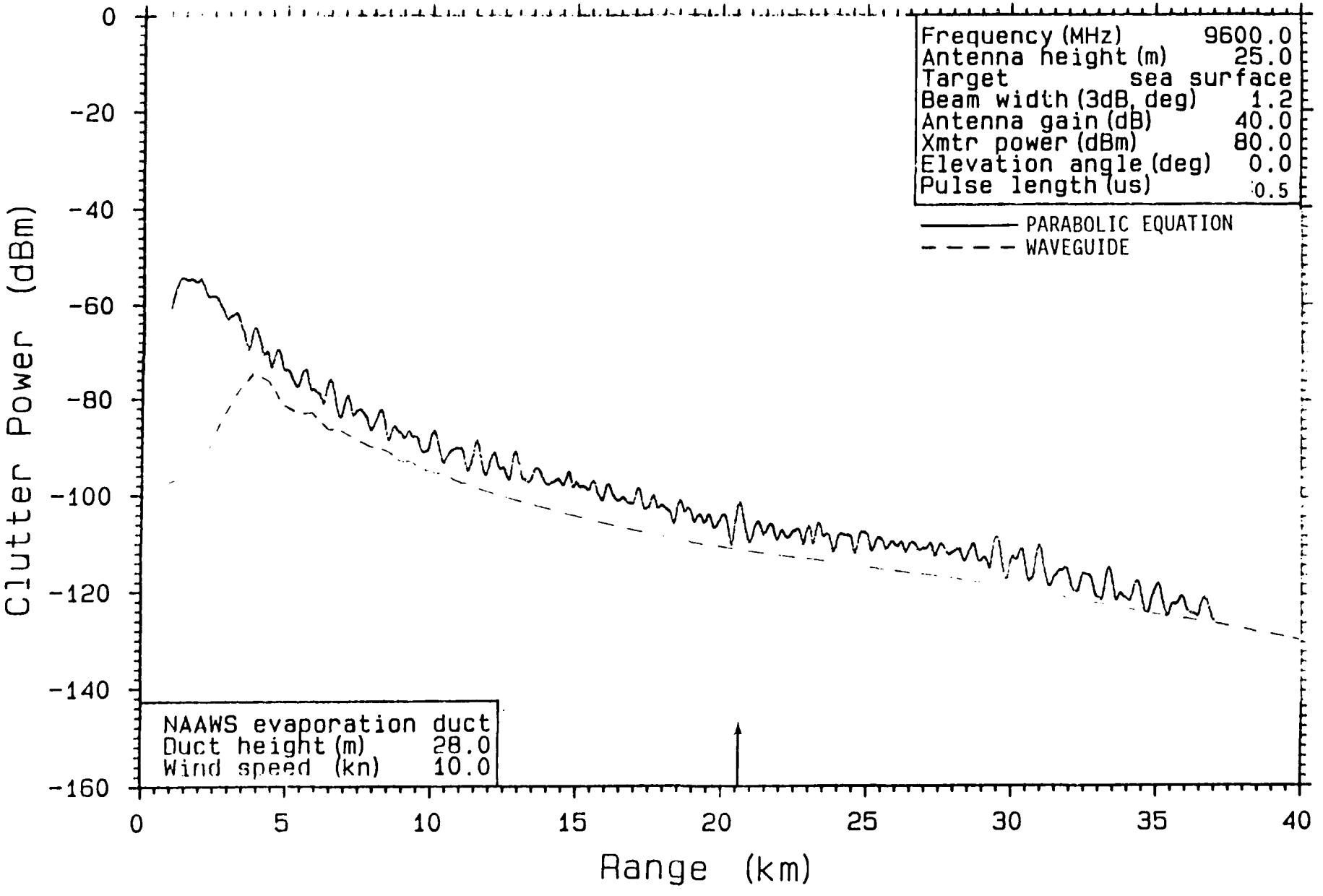

Figure 13. Clutter power vs. range. Comparison between pe and waveguide results. Twenty eight meter evaporation duct, 20 knot wind.

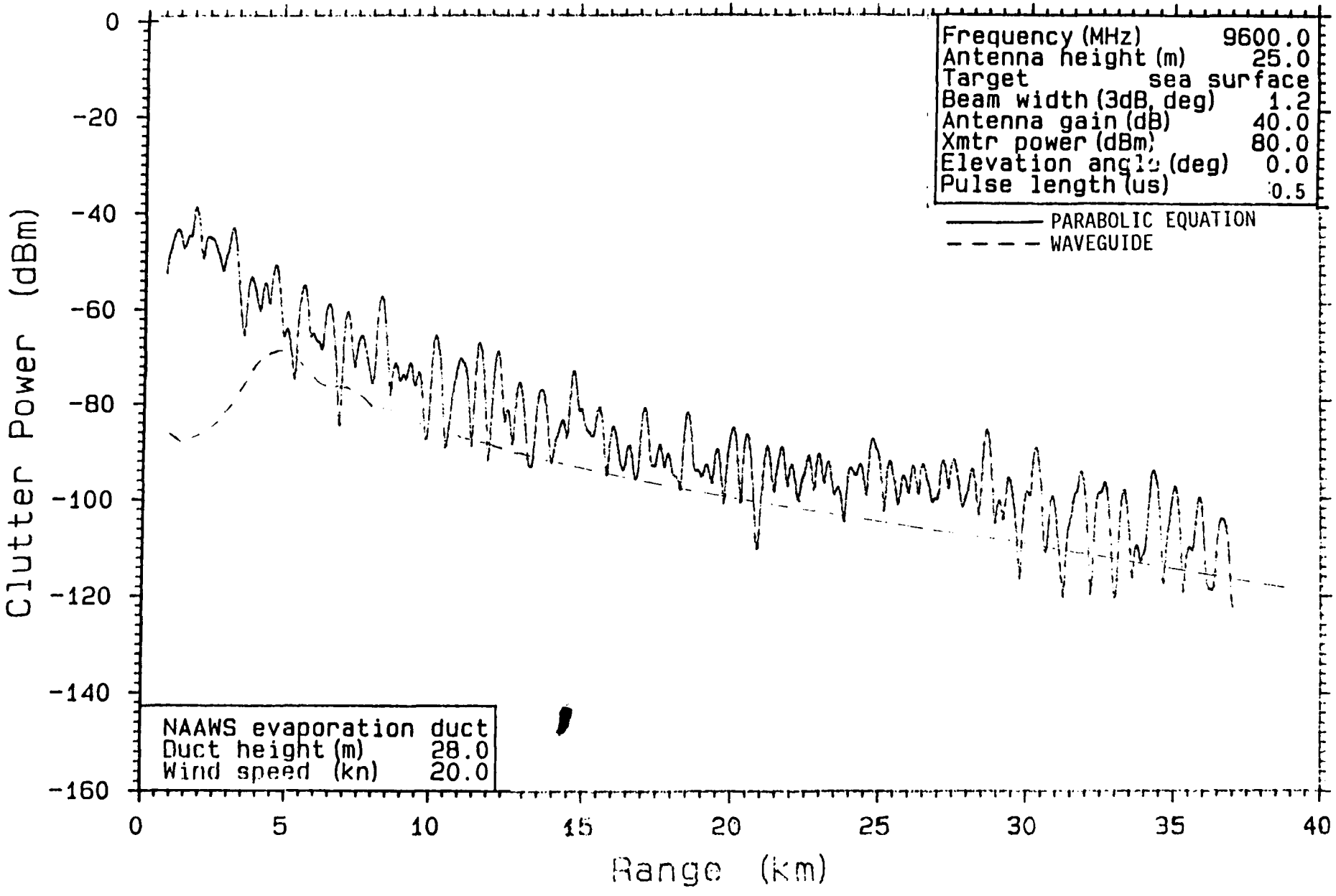

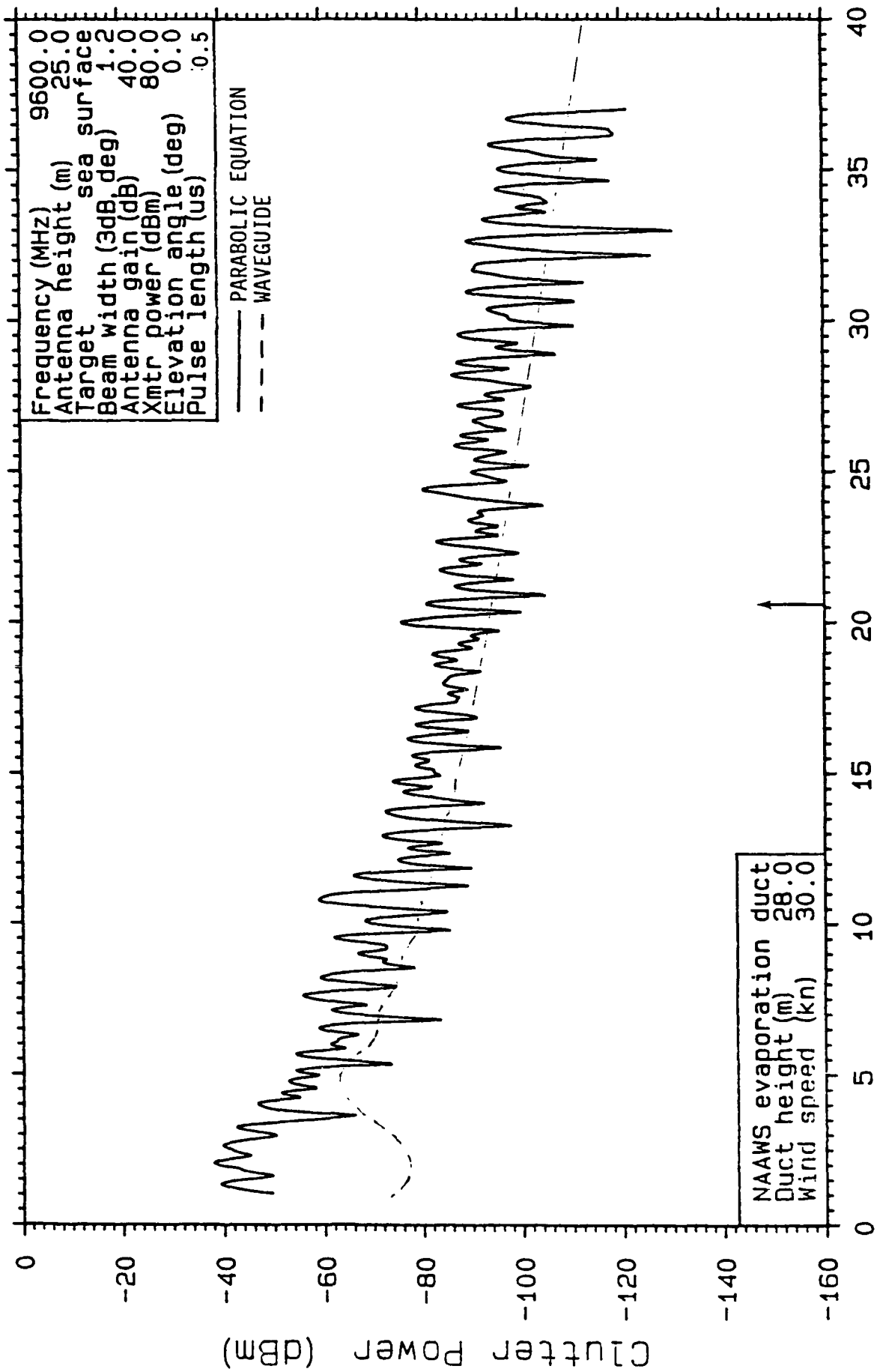

Figure 14. Clutter power vs. range. Comparison between pe and waveguide results. Twenty eight meter evaporation duct, 30 knot wind.

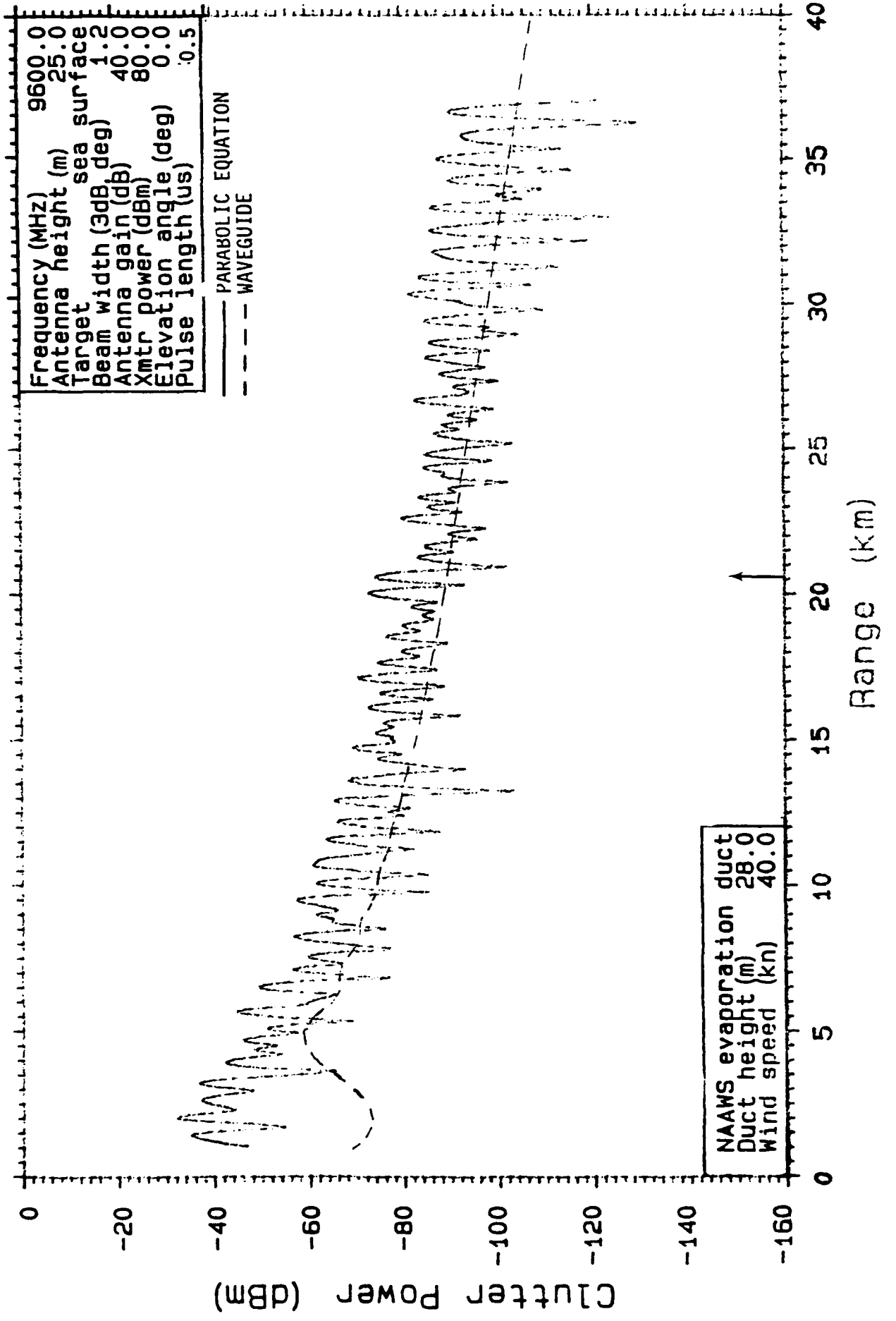

Figure 15. Clutter power vs. range. Comparison between pe and waveguide results. Twenty eight meter evaporation duct, 40 knot wind.

REPORT DOCUMENTATION PAGE

Form Approved
OMB No. 0704-0188

1. AGENCY USE ONLY *(Leave blank)*	2. REPORT DATE	3. REPORT TYPE AND DATES COVERED
	December 1989	Final

4. TITLE AND SUBTITLE

RADAR CLUTTER VIA WAVEGUIDE METHODS

5. FUNDING NUMBERS

PE: 0602435N
WU: DN488 760

6. AUTHOR(S)

R. A. Pappert

7. PERFORMING ORGANIZATION NAME(S) AND ADDRESS(ES)

Naval Ocean Systems Center
San Diego, CA 92152-5000

8. PERFORMING ORGANIZATION REPORT NUMBER

NOSC TD 1739

9. SPONSORING/MONITORING AGENCY NAME(S) AND ADDRESS(ES)

Office of Naval Technology
Arlington, VA 22217

10. SPONSORING/MONITORING AGENCY REPORT NUMBER

11. SUPPLEMENTARY NOTES

12a. DISTRIBUTION/AVAILABILITY STATEMENT

Approved for public release; distribution is unlimited.

12b. DISTRIBUTION CODE

13. ABSTRACT *(Maximum 200 words)*

Recent backscatter results generated by Tappert, using parabolic equation and Monte Carlo methods, afford an excellent opportunity to assess the adequacy of concepts such as shadowing and surface tilting often used in concert with ray concepts for line of sight backscatter calculations. In this study, results of first order scatter from rough surfaces are used in conjunction with waveguide formalism to calculate clutter from distant ranges in tropospheric waveguide environments. Comparisons are made with Tappert's results at 9.6 GHz for the standard atmosphere, and for 14 and 28 m evaporation ducts. Results apply to wind speeds of 10, 20, 30, and 40 knots. Averaged backscattered signals calculated by the two methods, for a transmitter altitude of 25 m, agree to within about $\pm$10dB. This is considered surprisingly good agreement in view of the many uncertainties and approximations involved in the calculations.

14. SUBJECT TERMS

backscatter calculations
waveguide methods

15. NUMBER OF PAGES

45

16. PRICE CODE

17. SECURITY CLASSIFICATION OF REPORT	18. SECURITY CLASSIFICATION OF THIS PAGE	19. SECURITY CLASSIFICATION OF ABSTRACT	20. LIMITATION OF ABSTRACT
UNCLASSIFIED	UNCLASSIFIED	UNCLASSIFIED	SAME AS REPORT